

# A study on phase sensitive imaging for breast tomosynthesis applications

Anastasia Daskalaki<sup>1</sup>, Gerasimos Messaris<sup>2</sup>, Nicolas Pallikarakis<sup>1</sup>

<sup>1</sup>Biomedical Technology Unit, School of Medicine, University of Patras, Greece

<sup>2</sup>Department of Medical Physics, University Hospital of Patras, Greece

SUBMISSION: 17/7/2019 | ACCEPTANCE: 29/11/2019

## ABSTRACT

**Purpose:** To examine the potential advantages of phase sensitive imaging in breast tomosynthesis (BT) for more accurate and early detection of breast cancer.

**Material and Methods:** An in-house phantom with a 5 cm radius and a 3 cm thickness of paraffin wax with embedded spheres, fibers and clusters of  $\text{CaCO}_3$ , simulating breast malignancies, was used. BT images were acquired with an in-line phase contrast mode using synchrotron radiation at 20 keV. Fifteen projections were obtained with an object to detector distance of 150 cm, acquisition arc of  $15^\circ$  and mean glandular dose (MGD) of 2.3 mGy. Attenuation based BT images of the same phantom were acquired with the use of a commercial imaging system. In this case,

15 projections were obtained at 28 kVp, 35 mAs with MGD 1.4 mGy, within an acquisition arc of  $15^\circ$ .

**Results:** In both experiments filtered back projection reconstruction algorithms were utilised, resulting in BT planes of 1 mm distance. The reconstructed planes of the two experiments were compared visually and quantitatively. The edges of the main mammographic structures appeared to be sharper in the case of phase contrast imaging, which made their detectability easier. Line profiles and contrast to noise ratio values confirmed the superiority of phase contrast BT over conventional BT imaging.

**Conclusions:** Tomosynthesis phase contrast imaging is a promising technique for the detection of small abnormalities in breast screening.



### KEY WORDS

Breast Tomosynthesis; Phase contrast imaging; Breast modeling; X-ray imaging Phantoms



### CORRESPONDING AUTHOR, GUARANTOR

Anastasia Daskalaki  
Biomedical Technology Unit, School of Medicine, University of Patras, 26500, Rio, Patras, Greece, Email: [dasnatasa@upatras.gr](mailto:dasnatasa@upatras.gr)

## 1. Introduction

While mammography is the most widespread screening tool for breast cancer, breast tomosynthesis (BT) is gaining ground in every day clinical practice. The problems caused by dense breast tissue, overlapping structures and thus structured noise in 2D mammography are significantly reduced in reconstructed tomosynthesis slices [1].

In BT imaging the x-ray source moves in a limited angle arc, providing a series of digital projection images of the breast [2-4]. These projections are then reconstructed into a stack of slices illustrating pseudo-3D structural information of the breast. The inherent disadvantage of conventional mammography to present superimposed structures in a single 2D image is resolved in BT [5]. BT may also result in greater accuracy for the size, shape and location of breast abnormalities and in more distinct illustration of abnormalities within dense breast tissue [6]. Tomosynthesis becomes a useful tool in the detection and depth localisation of breast abnormalities with dose levels not higher than those of conventional mammography [7]. Studies have shown that BT can also be beneficial in the characterisation of lesions particularly in dense breasts [8, 9] and has the potential to reduce the recall rate [10].

Recently phase contrast has been introduced as a promising x-ray imaging modality for the breast [11]. Conventional mammography and BT are imaging techniques based on the attenuation of the x-rays. Phase contrast (phase sensitive) imaging is a technique sensitive not only to attenuation but also to x-ray phase shift arising at the boundaries of different refractive materials [12, 13]. Tissues composed of low Z-elements, such as breast masses, produce low absorption contrast but considerable phase contrast, resulting in significant edge enhancement of structures [14-16]. It is worth mentioning that phase shift coefficients of tissues are greater than attenuation coefficients by two to three orders of magnitude, for x-rays in the diagnostic energy range. Additionally, phase shift coefficient diminishes less than attenuation coefficient as energy increases; thus, the potential application of phase contrast imaging with higher energies and lower delivered doses (an unrealistic approach in case of conventional mammography) is possible [17]. Among the different techniques under investigation nowadays for phase sensitive imaging, the in-line set up (free space

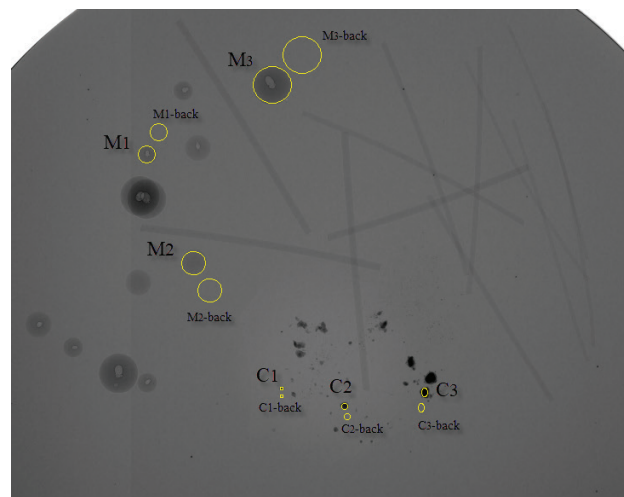


**Fig. 1.** ROIs under evaluation for the nylon spheres (M1, M2, M3) and for the specs of CaCO<sub>3</sub> (C1, C2, C3).

propagation imaging) is the most manageable and tested one. This approach does not require the use of any optics and grating elements in the imaging set-up between the sample and the detector, in order to perform wave splitting or any kind of image reconstruction [18-20].

In this study the potential advantages of BT combined with phase contrast imaging over conventional BT imaging were analysed. A relative comparison of BT slices generated by a commercial imaging system and by an in-line phase contrast set up with the use of synchrotron radiation was performed. For this comparison an in-house phantom was used, where the detectability and visualisation of structures simulating breast malignancies was evaluated.

## 2. Material and Methods

### 2.1. The Hardware Phantom

An in-house designed and made hardware phantom was used for the needs of the experiments. The phantom was made of paraffin wax (C<sub>25</sub>H<sub>52</sub>, density: 0.93 g/cm<sup>3</sup>, the real part of the refractive index decrement  $\delta_{(20\text{keV})} = 5.53 \cdot 10^{-7}$ ) mimicking a homogeneous background of 50% glandular-50% adipose tissue. It had a cylindrical form of 5 cm radius and 3 cm thickness inside which were embedded three different types of structures representing breast abnormalities: four groups of nylon spheres of 4.8 mm, 3.2 mm and 2.4 mm simulating masses, nylon fibers with sizes of 0.9 mm, 0.7 mm and 0.5 mm, and CaCO<sub>3</sub> powder simulating microcalcifications ( $\mu\text{Cs}$ ). During the solidification process four layers

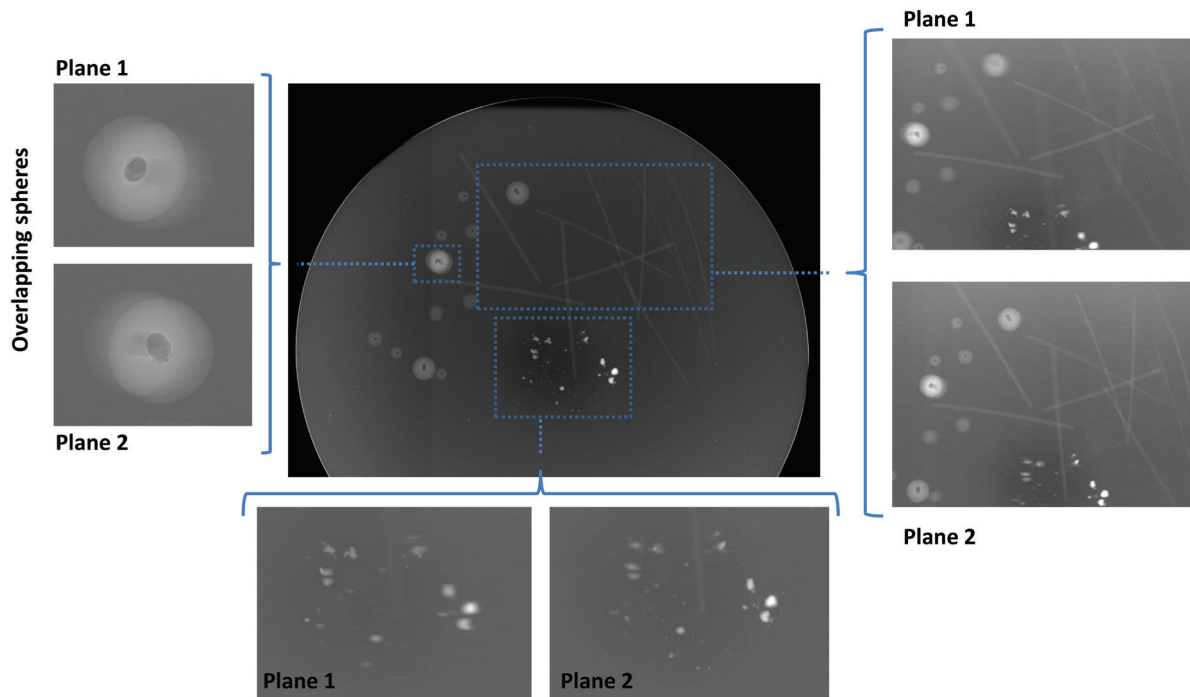


Fig. 2. Cropped phase contrast images illustrating spheres, fibers and CaCO<sub>3</sub> specs at two different in focus BT planes.

of the abovementioned structures were embedded. The aim of this arrangement was to produce areas with overlapping structures in order to facilitate a BT investigation. The phantom was tested in previous studies for phase contrast applications [21].

### 2.2. The Phase sensitive BT system

The experiment for phase sensitive imaging was performed at the Elettra Synchrotron at Trieste, using the SYNchrotron Radiation for MEDical Physics (SYRMEP) beamline, especially designed for research in medical diagnostic radiology. The optics were based on a double-crystal Si (111) monochromator working in the energy range of 18-35 keV. The detector was a Teledyne Dalsa Time Delay Integration (TDI) Charge-Coupled Device (CCD) camera with a pixel size of 54  $\mu\text{m}$ . The x-ray beam provided at 20 m from the source was a laminar section with maximum area 120 x 4 mm<sup>2</sup>. In order to acquire BT projections, the phantom was placed on a metal plate at 22.4 m from the source, moving vertically at each scan and able to rotate 360°. The object to detector distance (ODD) was 150 cm in a free space propagation set up. The energy of the monochromatic x-ray beam was 20 keV.

Projection images of 4400x2200 were produced within

an acquisition arc of 15° with 1° increment, resulting in 15 projections. Also a 2D image with the same acquisition parameters was obtained as a reference image for this experiment. The incident air kerma (K) was calculated in advance in order to acquire an MGD in the dose range of the European guidelines for quality assurance in breast cancer screening and diagnosing. For the calculations, the following equation was used:

$$MGD = K \times g \times c \times s \times t_{(g)} \quad (\text{Equation 1})$$

where  $g$ ,  $c$ , and  $t_{(g)}$  are conversion parameters depending on the breast thickness, the glandularity, the incident spectra and the angles of the acquisition arc respectively [22-25].  $K$  was measured at the upper surface of the breast and was equal to 0.4 R resulting in 3.45 mGy Entrance Surface Exposure (ESE). In our study, where the base material of the phantom was paraffin wax, the equivalent breast thickness was calculated and found to be 2 cm. According to Equation 1 the total MGD in this case was 2.3 mGy.

### 2.3. The Commercial BT system

In order to acquire attenuation based BT images, an

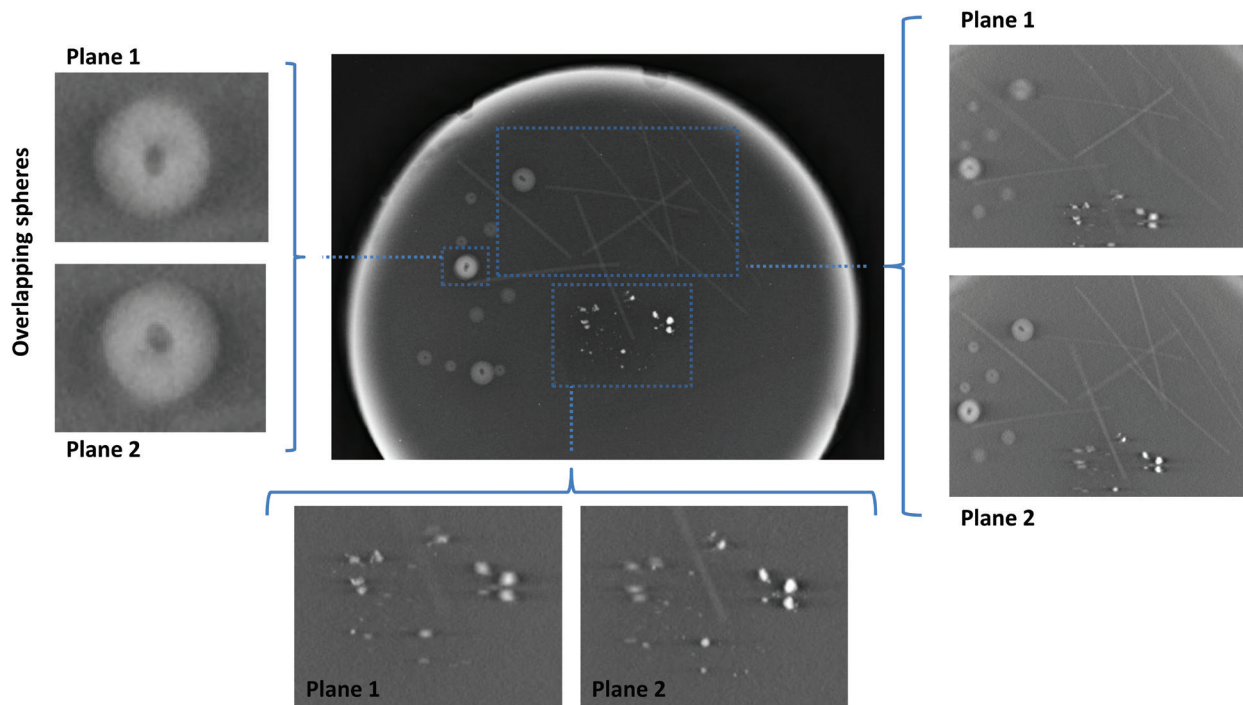


**Fig. 3.** Cropped attenuation based images illustrating spheres, fibers and  $\text{CaCO}_3$  specs at two different in focus BT planes.

experiment using the same phantom was carried out at the University Hospital of Patras with the use of a commercial system (Selenia Dimensions, Hologic) [26]. The imaging system had a flat panel amorphous selenium detector with an image receptor size of  $24 \times 29$  cm ( $3328 \times 4096$ ) and pixel size of  $70 \mu\text{m}$ . The x-ray tube had a Tungsten anode with  $0.3$  mm focal spot size. The projections were taken with an automatic exposure control (AEC) mode where the system selects filter, kVp and mAs. In our case an Al filter of  $0.7$  mm,  $28$  kVp and  $35$  mAs was used. Fifteen projections in  $15^\circ$  acquisition arc were obtained with an OOD of  $5.8$  cm and a source to detector distance of  $70$  cm. Also a 2D image with the same acquisition parameters was obtained as a reference image, alike in the previous experiment. The isocenter of this imaging system was in the detector that rotated making small moves. The ESE was derived from the imaging system and was equal to  $2.45$  mGy. The total MGD was calculated with the same Equation 1 and found to be  $1.4$  mGy.

#### 2.4. Image processing and reconstruction

Before reconstruction, a flat-field correction was performed to the projection images acquired with the

in-line phase contrast BT set up. Additional processing was performed using MATLAB 2013 in order to correct the small vertical movements of the phantom during the BT acquisition arcs. For the reconstruction process an in-house platform was used [27] performing filtered back-projection. All the images were pre-filtered with the use of ramp filter. A pseudo-3D representation of the phantom was produced from the reconstructed axial planes at every  $1$  mm of the total volume. Windowing methods were used in order to obtain the best image quality regarding the visualisation of the structures inside the phantom. There was no extra filtration or any other post processing of the images before visual comparison.

#### 2.5. Evaluation metrics for comparison

The reconstructed phase sensitive and attenuation images were compared visually and quantitatively. For visual assessment, five investigators familiar with medical imaging from our research group were involved. For the quantitative analysis evaluation metrics were used. In this study the Contrast to Noise Ratio (CNR) was calculated [28, 29] for the main mammographic findings (Nylon spheres and  $\text{CaCO}_3$  specs) according to Equation 2,

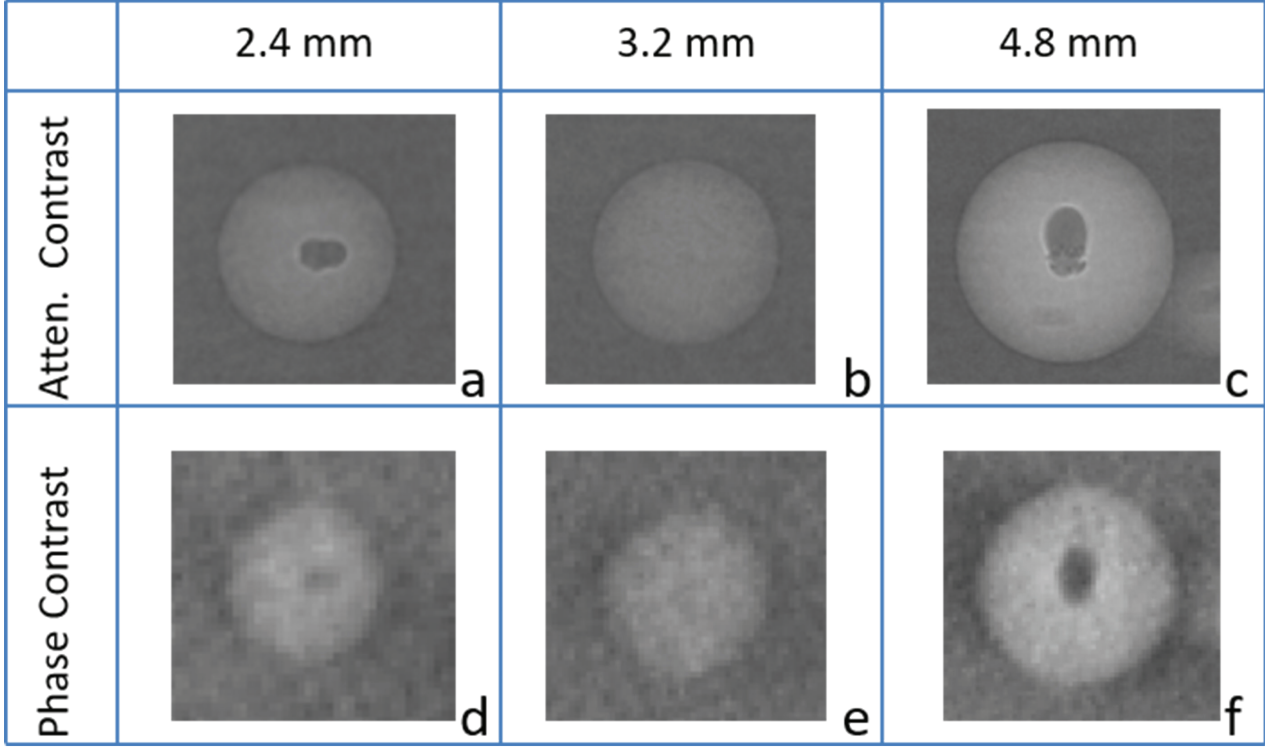


Fig. 4. Cropped images of spheres in focus with different sizes from phase contrast BT planes (a, b, c) and from attenuation contrast BT planes (d, e, f).

$$CNR = \frac{I_o - I_B}{\sqrt{\frac{\sigma_o^2 + \sigma_B^2}{2}}} \times \sqrt{\alpha_o / \alpha_p} \quad (\text{Equation 2})$$

where  $I_o$  and  $I_B$  are the average intensity values of the object and background over a region of interest (ROI),  $\sigma_o$  and  $\sigma_B$  are the standard deviation values of the object and background ROI and  $\alpha_o$  and  $\alpha_p$  are the areas of the object and a pixel respectively.

The ROIs used were circular with altered sizes according to the size of each object under investigation (Fig. 1). M and C denote the ROIs for spheres and  $\text{CaCO}_3$  specs respectively. For each structure under evaluation a background ROI was used, of the same size with the object's ROI. The background ROIs were placed in the neighbourhood of each object, where no details appeared.

$$FOM = \frac{CNR^2}{MGD} \quad (\text{Equation 3})$$

Since the two experiments were performed with different doses and CNR values were depending on the radiation dose, a figure of merit (FOM) was introduced. In order to allow the comparison of CNR between the two experiments FOM values were calculated, where

the  $CNR^2$  was normalised to the MGD according to Equation 3 [30].

### 3. Results

The reconstructed BT planes for phase sensitive and attenuation imaging were compared visually and quantitatively in means of CNR, FOM and line profiles. As we sliced through the reconstructed volume of 30 planes, different structures appeared in focus. In Fig. 2 a 2D image acquired with the in-line phase contrast set up is illustrated. Cropped images of spheres, fibers and  $\text{CaCO}_3$  specs from areas of the phantom defined with dashed lines are demonstrated. Those images were cropped from 2 different planes (plane 1 and plane 2) out of the 30 that were reconstructed. Fig. 3 illustrates the same areas with Fig. 2, but attenuation based BT reconstructed planes acquired with the commercial imaging system were used.

In Fig. 4, which is dedicated to the low contrast features of the phantom, nylon spheres simulating breast masses with different diameters are illustrated. In the first row (Fig. 4a, b, c) cropped images of spheres with increasing diameter sizes of 2.4 mm, 3.2 mm and

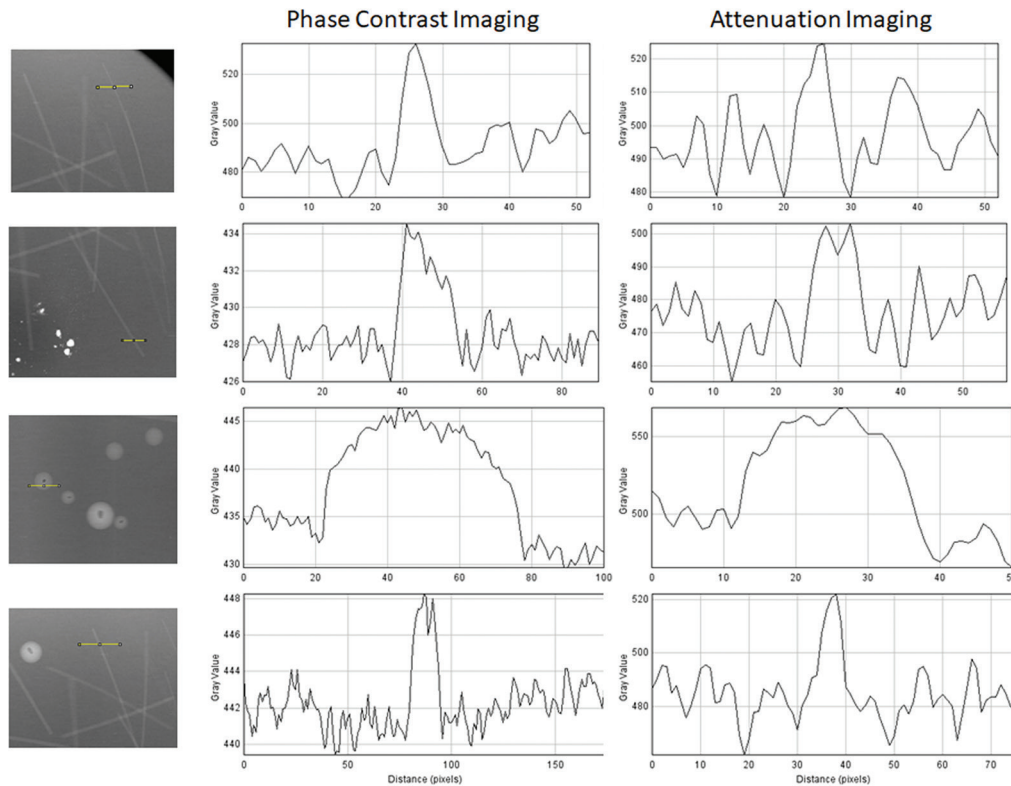


**Fig. 5.** Line profiles taken across fibers and one sphere from phase contrast and attenuation BT planes.

4.8 mm from phase contrast in-focus BT planes are presented. Whereas in the second row (Fig. 4d, e, f) the same spheres are presented, appearing in-focus in attenuation contrast BT planes.

In Fig. 5, line profiles for fibers and for one sphere in both imaging cases are highlighted. The first column from the left shows cropped images of the areas where the line profiles denoted with yellow lines were obtained. In the middle and third column are the line profiles obtained across phase sensitive reconstructed planes and attenuation based reconstructed planes respectively.

In Table 1 the calculated values of CNR and FOM according to Equations 2 & 3 for three nylon spheres and three CaCO<sub>3</sub> specs for the two different imaging modalities are listed. The ROIs used for those calculations are presented in Fig. 1.

**4. Discussion**

This study investigated the potential enhancement of image quality in the case of phase sensitive BT imaging over conventional BT. Experiments were performed with a commercial BT system for attenuation imaging

**Table 1.** Calculated values of CNR and FOM for the spheres (M1, M2, M3) and for CaCO<sub>3</sub> specs (C1, C2, C3)

	Phase Sensitive Imaging		Attenuation Imaging	
	CNR	FOM	CNR	FOM
<b>M1</b>	6.32	17.39	4.23	12.75
<b>M2</b>	7.59	25.04	4.75	16.15
<b>M3</b>	7.27	23.00	5.12	18.74
<b>C1</b>	14.70	93.95	11.03	86.87
<b>C2</b>	12.81	71.30	8.36	62.59
<b>C3</b>	10.59	48.73	6.31	28.48

and an in-line phase contrast BT set up with synchrotron radiation for phase sensitive imaging. An in-house phantom tested in previous experiments was used in both experiments with low and high contrast features mimicking breast abnormalities embedded into the base material.

Both BT cases managed to resolve areas with overlapping structures, providing better localisation and characterisation of those features. This can be seen

in areas of the phantom with spheres and fibers (Fig. 2 and Fig. 3 on the right). This is evident in the example of two superimposed spheres that in both BT modalities appeared in-focus in two separate reconstructed planes (Fig. 2 and Fig. 3 on the left). This advantage of in depth localisation of features that BT provides might be helpful in biopsy guidance and breast operation planning.

The detectability of the mammographic findings of the phantom from the two imaging modalities was evaluated visually and quantitatively. Visual assessments of the reconstructed slices showed superiority in the case of phase contrast BT. The nylon spheres mimicking masses with different diameters appeared in the phase sensitive images with sharper edges compared to those of conventional ones (Fig. 4). As seen in Fig. 4d-f, for attenuation contrast images the decrease in the size of the spheres resulted in inferior detectability of those features. Especially the sphere of 2.4 mm diameter (Fig. 4d) is not easily distinguished among the homogeneous background. In phase contrast images, the spheres appear sharper with more intense edge enhancement and even the smallest one is clearly depicted (Fig. 4a). The same stands for the fibers. However, for the  $\text{CaCO}_3$  specs visually identified differences were not significant between the two modalities.

The diagnostic approach to breast calcifications is to analyse the morphology, distribution and sometimes change over time. The form or morphology of calcifications is the most important factor in deciding whether they are typically benign or of suspicious morphology according to Bi-RADS 2013 [31]. Also masses can be categorised according to their margins and shape. The superiority of phase sensitive BT in visualising stronger edge enhancement might be critical for the characterisation of breast abnormalities.

The results of visual assessments come in agreement with the quantitative analysis. Line profiles taken across three fibers and one sphere (Fig. 5) indicated superiority of phase contrast BT over conventional BT in the detectability of these features. Line profiles of

this modality clearly show the position of the fibers and the sphere inside the phantom. This clear appearance of a structure over the background, in the case of phase sensitive BT images, is due to the edge-enhancement effect. This outcome could provide ancillary information for digital segmentation applications and for computer-aided detection. Moreover, conventional BT planes suffer from background noise (quantum noise) and one of the reasons could be the lower dose level used.

The improved image quality of phase contrast BT over conventional BT is confirmed by the CNR and FOM values presented in Table 1. Low and high contrast features exhibited higher FOM values in phase sensitive BT. This is an important result for breast imaging, since the enhanced contrast of low contrast features as well as the clear visualisation of  $\text{CaCO}_3$  specs is desired. As expected, high contrast features demonstrated significantly higher values of CNR and FOM compared to low contrast features in both imaging cases. For the nylon spheres, and as their diameter increased from M1 to M3, the FOM values increased. The opposite stands for the  $\text{CaCO}_3$  specs, where the increase of their size from C1 to C3 resulted in decreased FOM values. This could be a result of the smaller ROI size that for specs varied from 12 to 104 pixels, whereas for spheres varied from 911 to 4250 pixels.

Synchrotron radiation performance has been found to be advantageous for phase sensitive imaging; however its use is limited for research. Therefore, in the future, alternative types of phase contrast imaging that could be applicable in clinical settings should also be studied and evaluated. **R**

### **Conflict of interest**

*The authors declared no conflicts of interest.*

### **Acknowledgements**

**Funding:** This research has been co-financed by the Greek State Scholarship Foundation (I.K.Y.) through the Operational Program “Education and Lifelong Learning”.

## REFERENCES

1. Sechopoulos I. A review of breast tomosynthesis. Part II. Image reconstruction, processing and analysis, and advanced applications. *Med Phys* 2013; 40(1): 014302.
2. Sechopoulos I. A review of breast tomosynthesis. Part I. The image acquisition process. *Med Phys* 2013; 40(1): 014301.
3. Pisano ED, Yaffe MJ. Breast cancer screening: Should tomosynthesis replace digital mammography: *JAMA* 2014; 311(24): 2488-2489.
4. Park JM, Franken EA Jr, Garg M, et al. Breast tomosynthesis: present considerations and future applications. *Radiographics* 2007; 27(Suppl 1): S231-240.
5. Dobbins JT III, Godfrey DJ. Digital x-ray tomosynthesis: current state of the art and clinical potential. *Phys Med Biol* 2003; 48: R65-R106.
6. Phi XA, Tagliafico A, Houssami N, et al. Digital breast tomosynthesis for breast cancer screening and diagnosis in women with dense breasts - a systematic review and meta-analysis. *BMC Cancer* 2018; 18(1): 380.
7. Niklason LT, Christian BT, Niklason LE, et al. Digital tomosynthesis in breast imaging. *Radiology* 1997; 205: 399-406.
8. Pan HB, Wong KF, Yao A, et al. Breast cancer screening with digital breast tomosynthesis - 4 year experience and comparison with national data. *J Chin Med Assoc* 2018; 81(1): 70-80.
9. Gong X, Glick SJ, Liu B, et al. A computer simulation study comparing lesion detection accuracy with digital mammography, breast tomosynthesis, and cone-beam CT breast imaging. *Med Phys* 2006; 33: 1041-1052.
10. Bernardi D, Li T, Pellerrini M, et al. Effect of integrating digital breast tomosynthesis (3D-mammography) with acquired or synthetic 2D-mammography on radiologists' true-positive and false-positive detection in a population screening trial: A descriptive study. *Eur J Radiol* 2018; 106: 26-31.
11. Castelli E, Tonutti M, Arfelli, et al. Mammography with synchrotron radiation: first clinical experience with phase-detection technique. *Radiology* 2011; 259(3): 684-694.
12. Bravin A, Coan P, Suotti P. X-ray phase contrast imaging: from preclinical applications towards clinics. *Phys Med Biol* 2013; 58: R1-R35.
13. Bliznakova K. Application of Synchrotron Radiation in Mammography. *Recent Pat Med Imaging* 2012; 2: 94-110.
14. Sarno A, Mettivier G, Golosio B, et al. Imaging performance of phase-contrast breast computed tomography with synchrotron radiation and a CdTe photon-counting detector. *Physica Med* 2016; 32(5): 681-690.
15. Wu X, Liu H. Clinical implementation of X-ray phase-contrast imaging: Theoretical foundations and design considerations. *Med Phys* 2003; 30(8): 2169-2179.
16. Olivo A, Rigon L, Vinnicombe SJ, et al. Phase contrast imaging of breast tumours with synchrotron radiation. *Appl Radiat Isot* 2009; 67: 1033-1041.
17. Wong MD, Yan A, Ghani M, et al. Dose and detectability improvements with high energy phase sensitive x-ray imaging in comparison to low energy conventional imaging. *Phys Med Biol* 2014; 59(9): N37.
18. Bliznakova K, Russo P, Kamarianakis Z, et al. Inline phase-contrast breast tomosynthesis: a phantom feasibility study at a synchrotron radiation facility. *Phys Med Biol* 2016; 61(16): 6243.
19. Baran P, Pacile S, Nesterets YI, et al. Optimization of propagation-based x-ray phase-contrast tomography for breast cancer imaging. *Phys Med Biol* 2017; 62(6): 2315.
20. Wu X, Liu H. Clinical implementation of X-ray phase-contrast imaging: Theoretical foundations and design considerations. *Med Phys* 2003; 30(8): 2169-2179.
21. Daskalaki A, Pallikarakis N. Image quality evaluation of phase contrast mammographic techniques. *IFMBE proceedings* 2018; 68(1): 9-13.
22. Dance DR, Skinner CL, Young KC, et al. Additional factors for the estimation of mean glandular breast dose using the UK mammography

- dosimetry protocol. *Phys Med Biol* 2000; 45: 3225-3240.
23. Dance DR, Young KC, van Engen RE. Estimation of mean glandular dose for breast tomosynthesis: Factors for use with the UK, European, and IAEA breast dosimetry protocols. *Phys Med Biol* 2011; 56: 453-471.
24. Suleiman ME, Brennan PC, McEntee MF. Mean glandular dose in digital mammography: a dose calculation method comparison. *J Med Imaging (Bellingham)* 2017; 4(1): 013502.
25. Dance DR, Young KC, van Engen RE. Further factors for the estimation of mean glandular dose using the United Kingdom, European and IAEA breast dosimetry protocols. *Phys Med Biol* 2009; 54: 4361-4372.
26. Selenia Dimensions Mammography Systems. Available via [guttaeu.eu/wp-content/uploads/2017/11/SeleniaDimensions.pdf](http://guttaeu.eu/wp-content/uploads/2017/11/SeleniaDimensions.pdf).
27. Kamarianakis Z, Buliev I, Pallikarakis N. A platform for Image Reconstruction in X-ray Imaging: Medical Applications using CBCT and DTS algorithms. *Computer Science Journal of Moldova* 2014; 22(2)(65): 236-252.
28. Ghani M, Wu D, Li Y, et al. Quantitative analysis of contrast to noise ratio using a phase contrast x-ray imaging prototype. In: *Biophotonics and Immune Responses VIII* 2013; 8582: 85820H.
29. Ghani MU, Wong MD, Omoumi FH, et al. Detectability comparison of simulated tumors in digital breast tomosynthesis using high-energy X-ray inline phase sensitive and commercial imaging systems. *Physica Medica* 2018; 47: 34-41.
30. Borg M, Badr I, Royle GJ. The use of a figure-of-merit (FOM) for optimisation in digital mammography: a literature review. *Radiat Prot Dosimetry* 2012; 151(1): 1-8.
31. Zonderland H, Smithuis R. Bi-RADS for Mammography and Ultrasound 2013. Updated version. Available via [radiologyassistant.nl/breast/bi-rads-for-mammography-and-ultrasound-2013](http://radiologyassistant.nl/breast/bi-rads-for-mammography-and-ultrasound-2013). Published October 08, 2014.



READY - MADE  
CITATION

Daskalaki A, Messaris G, Pallikarakis N. A study on phase sensitive imaging for breast tomosynthesis applications. *Hell J Radiol* 2019; 4(4): 18-26.